



# Shell Model Study of the Neutron-Rich Nuclei around N=28

J. Retamosa\*, E. Caurier\*, F. Nowacki\*\* and A. Poves\*\*\*

CRN IN2P3-CNRS/Université Louis Pasteur BP20

F-67037 Strasbourg-Cedex, France.

\*\* GANIL IN2P3-CNRS BP5027

F-14021 Caen-Cedex, France

\*\*\* Departamento de Física Teórica C-XI

Universidad Autónoma de Madrid

E-28049 Madrid, Spain.

(August 11, 2018)

We describe the properties of the neutron rich nuclei around N=28 in the shell model framework. The valence space comprises the *sd* shell for protons and the *pf* shell for neutrons without any restriction. Good agreement is found with the available experimental data. The N=28 shell closure, even if eroded due to the large neutron excess, persists. The calculations predict that  $^{40}\text{S}$  and  $^{42}\text{S}$  are deformed with  $\beta = 0.29$  and  $\beta = 0.32$  respectively.

## I. INTRODUCTION

The exploration of the behaviour of the nucleus under extreme conditions; high spin, vicinity to the drip lines, finite temperature, etc. is a major source of new insights in nuclear structure. One of the most important questions raised by the study of the drip lines is whether the basic shell order evolves with the neutron (proton) excess. An example of this problem is given by the N=20 very neutron rich nuclei where the strong anomalies detected [1–4] were explained as a collapse of the standard N=20 shell closure. Extended shell model calculations [5–7] showed that the inversion of the spherical closed-shell configurations and the 2p-2h collective intruders could account for the large binding energies and half-lives, unexpected ground-state spins, and high level densities at low excitation energies. Also, mean-field calculations using the Skyrme interaction predicted a sharp transition from spherical to prolate shapes [8]

Recently, there has been an increase of interest in the N=28 isotones far from the stability, motivated by; i) the possible existence of anomalies in the shell closures, as already found in N=20 and ii) the unusual  $^{48}\text{Ca}/^{46}\text{Ca}$  abundance ratio measured in the solar system or the Ca-Ti-Cr anomalies observed in some meteoritic inclusions.

Sorlin et al. [9] undertook the study of the  $\beta$ -decay and  $\beta$ -delayed neutron emission probabilities for  $^{44}\text{S}$  and  $^{45-47}\text{Cl}$ . Their measured half-lives were much larger than those predicted by TDA [10] or QRPA [11] calculations. These discrepancies were attributed to unexpected shape transitions in the region. Mass formulas such as the finite-range liquid drop [12], the finite-range droplet [13] or the Extended Thomas-Fermi with shell corrections [14] predict the existence of shape coexistence around  $^{44}\text{S}$ . In all the cases the energy surfaces are very soft with close lying minima corresponding to different deformations.

Similar conclusions have been drawn by Werner et al [15]. Relativistic mean field calculations and non-relativistic ones using the Skyrme forces produce very flat energy surfaces for the Sulphur isotopes, with several minima separated by energy barriers of just a few hundred keV. In this situation it seems necessary to go beyond the mean-field using, for instance, the generator coordinate method.

In this paper we discuss all the neutron rich nuclei with  $N \geq 20$  and  $14 \leq Z \leq 20$  in the Shell Model framework. This is, to some extent, complementary to the other methods mentioned above and can give new information on the structure of these nuclei. The paper is organized as follows. Section II gives a brief description of the model, discussing the choice of the valence space, the effective interaction and the coulomb corrections. Section III compares our results with the experimental data. In section IV we examine the behaviour of the N=28 shell closure far from the stability. Section V deals with deformation in heavy Sulphur isotopes.

## II. THE MODEL

### A. The Valence Space

It consists of the full *sd* shell for Z-8 protons and the full *pf* shell for N-20 neutrons. Although the calculations reach very large dimensionalities, they can be performed without truncations in all cases. We do not include the intruder states that could be formed by exciting particles from the *sd* to the *pf* shell. These kind of states, that appear at low excitation energy around  $^{40}\text{Ca}$ , should be less important near N=28. The reason is twofold; *sd* protons get more

and more bound with increasing neutron excess than unfavouring proton intruders; and the correlation energy of the configurations with neutron intruders do not gain much energy compared to the standard ones (the opposite is true in e.g.  $^{32}\text{Mg}$ ). This is in agreement with the observed spectra. The existence of many collective low lying states near  $N=Z=20$  contrast with their absence for  $N \simeq 28$ ,  $Z > 20$ .

## B. The interaction

The construction of the effective hamiltonian is critical in any shell model description. It is well known that the saturation properties of the realistic interactions must be corrected phenomenologically in order to have a good description of the nuclear structure [17]. Unfortunately, the experimental data for the very neutron rich nuclei with  $14 \leq Z \leq 18$  are scarce. Even if the masses are known over a relatively wide region, at  $N=28$  they have only been measured for nuclei with  $Z \geq 19$ . As an example the masses of the Sulfur isotopes are only known up to  $N=26$ . Half-lives are only known for  $^{44}\text{S}$  and  $^{45-47}\text{Cl}$ . The level schemes of Ar and Cl with  $20 \leq N \leq 23$  are partly established. The situation is clearly better for the K isotopes where the evolution of the  $3/2^+, 1/2^+$  doublet with the neutron number is known up to  $N=28$  [18].

Our starting interaction has three parts. The USD interaction of Wildenthal [19] is used for the particles lying in the sd-shell. A modified version of the Kuo-Brown interaction, denoted  $\text{KB}'$  in ref [20], gives the two body matrix elements for the  $pf$  shell particles. This interaction is better suited to this valence space than the  $\text{KB3}$  interaction that has been used in conventional  $pf$  shell calculations [24]. Furthermore, when used in the lower part of the  $pf$  shell it also gives good spectroscopic results. Finally, the cross-shell interaction is the G-matrix of Lee, Kahanna and Scott (LKS) [21]. This is the part of the interaction whose monopoles we have proceeded to modify phenomenologically. The data used in the fit are:

- The natural parity states of nuclei with few  $pf$  particles and sd holes.
- The evolution of the  $3/2^+, 1/2^+$  doublet along the K isotopes.
- The position of the  $5/2^+$  states in  $^{47}\text{K}$ .

The experimental data cited above are not enough to fix all the monopole parameters. They essentially fix the interaction among neutrons in the  $1f_{7/2}$  and  $2p_{3/2}$  orbits with the  $sd$  protons. On the contrary, the interaction with  $1f_{5/2}$  and  $2p_{1/2}$  particles is not well determined. In our choice of the final interaction  $^{41}\text{Ca}$  and  $^{35}\text{Si}$  have very similar single neutron spectra as predicted in Duflo and Zuker [22] mass formula. There exists other possible choices of this part of the interaction that induce important modifications in the structure of heavy Silicons and to a minor extent in that of the heavy Sulphurs.

The 2-body matrix elements incorporate a tiny mass dependence and are written as:

$$V = \frac{\omega(A)}{\omega(A_0)} V_0 = \frac{\langle r^2(A_0) \rangle}{\langle r^2(A) \rangle} V_0 \quad (1)$$

where  $A_0 = 40$  and  $\hbar\omega_0=11$  MeV are used to calculate the LKS G-matrix. Instead of the usual law  $\langle r^2 \rangle = r_0 A^{1/3}$  fm, we borrow from reference [22] a modified expression, which is better adapted to large mass regions.

$$\langle r^2 \rangle = r_0 \left[ A \left( 1 - \zeta \left( \frac{N-Z}{A} \right)^{1/2} \right) \right]^{1/3} . \quad (2)$$

leading to the following expression for the 2-body matrix elements

$$V = \left[ \left( \frac{A_0}{A} \right) \left( 1 - \zeta \left( \frac{N-Z}{A} \right)^{1/2} \right) \right]^{1/3} V_0 \quad (3)$$

with  $\zeta = 0.42$  and  $A_0 = 40$ .

### C. Coulomb Energies

The absolute energies predicted with the precedent interaction are relative to an  $^{16}\text{O}$  core and do not include the coulomb energy of the protons. Thus, to compare our predictions with the experiment, they must be corrected with the following prescription:

$$E_i(N, Z) = E_0 + E_c(N, Z) + E_i^{SM}(N, Z) \quad (4)$$

where  $E_0$  is the inert core energy (127.62 MeV),  $E_c(N, Z)$  is the coulomb energy relative to the core and  $E_i^{SM}$  is the nuclear energy obtained with our interaction. The  $E_c$  energy, which is assumed to depend only on N and Z, has been calculated with the Antony and Pape formula [23]

$$E_c(A, Z) = \begin{cases} E_c(A, Z - 1) + 1.44(Z - 1/2)/A^{1/3} - 1.02 & Z > Z_s \\ E_c(A, Z + 1) - 1.44(Z + 1/2)/A^{1/3} + 1.02 & Z < Z_s \end{cases} \quad (5)$$

where  $Z_s = A/2$  or  $(A + 1)/2$  and the coulomb correction  $E_c(Z_s)$  along the stability line is given by

$$E_c(Z_s) = \begin{cases} 0.162Z^2 + 0.95Z - 18.25 & Z \leq 20 \\ 0.125Z^2 + 2.35Z - 31.53 & Z > 20 \end{cases} \quad (6)$$

which agrees with the Chung-Wildenthal coulomb correction [6] when  $Z_s \leq 20$  and with that of reference [24] for  $Z_s > 20$ .

## III. RESULTS AND DISCUSSION

### A. Comparison with the data.

In this section we compare the theoretical predictions with the experimental data. The shell model matrices are dealt with by the code *ANTOINE* [25] a very fast and efficient implementation of the Lanczos algorithm. The USD predictions for the *sd*-shell nuclei have been largely reported [19]. However, we shall include *sd* nuclei in the  $S_{2N}$  plots to stress the continuity of the shell model description across the N=20 magic number.

Table I, contains the predicted and experimental energies of the  $2^+$  states, that show an excellent agreement. The interaction, adjusted to reproduce the behaviour of the  $3/2^+$ ,  $1/2^+$  levels along the odd-A K, predicts for the doublet a similar behaviour in the neutron rich Chlorine and Phosphorous (see table II). The crossing of these two levels is due to the gradual degeneracy of the  $2s_{1/2}$  and  $1d_{3/2}$  orbitals as the occupation of the  $1f_{7/2}$  shell increases. In the P isotopes, the  $1d_{5/2}$  orbit is nearly closed, consequently the evolution of the doublet gives us an idea of the relative position of the two orbitals. As we shall comment later, their relative position is determinant for the development of deformation in the heavy Sulphurs.

The spectroscopic information on the nuclei with  $Z < 20$   $N > 20$  is limited to a some K, Ar and Cl isotopes. Figures 1 to 7 show the theoretical and experimental spectra for the cases  $^{40-42}\text{K}$ ,  $^{39-41}\text{Ar}$  and  $^{38}\text{Cl}$  for which the energy levels are known. Yet, there are still many uncertainties in the measured level schemes, specially the spin assignments. The theory-experiment agreement is perfect for  $^{40-41}\text{K}$  and  $^{40}\text{Ar}$ . The few states without theoretical counterpart are most probably *sd*-intruders. For the other nuclei the concordance is also quite good.

In addition to these spectra, the half-lives of several Ar and S isotopes are known. Their decays are dominated by allowed Gamow Teller transitions. The ground states of the father nuclei were calculated in our  $0\hbar\omega$  space and the Gamow-Teller sum rule state was determined in a larger space that includes all the  $1p - 1h$  in order to recover the  $3(N - Z)$  sum rule. The strength functions were obtained by the Whitehead method [26]. The phase space factors of Wilkinson [27] were used to compute the half-lives. Total strengths and half-lives are compiled in table III. The agreement is very satisfactory. The calculated half-life of  $^{44}\text{S}$  is very sensitive to the  $Q_\beta$ . We have used the theoretical value; if we had employed the extrapolated number given in the Audi and Wapstra compilation [29], the half-life would have increased to 150ms.

The two neutron separation energies  $S_{2N}$  are known over a large region, unfortunately, for most Z's they do not reach N=28. The agreement with the experimental results is good as it can be seen in figures 8 to 12. However, the discrepancies with the extrapolated masses [29] are important.

## B. Does the N=28 shell gap persist?

To answer to this question we analyse our predictions for the  $S_{2N}$ , the excitation energies of the first  $2^+$  states, and the occupation numbers. Structural changes, such as spherical to deformed shape transitions, should show up in the behaviour of these quantities as a function of the neutron number.

The  $S_{2N}$ 's around N=28 have some common features for different Z-values. In three cases: Ca, K and Si, a sharp decrease of  $S_{2N}$  is observed at N=28. For the other isotopes, there are not sharp slope changes, but  $S_{2N}$  still decreases. These results are consistent with a shell closure. This conclusion is opposite to that coming from the mass systematics, that predicts almost constant  $S_{2N}$  around N=28, and that could be interpreted as a signature of a new region of deformation.

Figure 13 shows the evolution of the  $2^+$  energy for the Ca and Si isotopes. The large energy increase of the  $2^+$  for the four nuclei  $^{40}\text{Ca}$ ,  $^{48}\text{Ca}$ ,  $^{34}\text{S}$  and  $^{42}\text{Si}$  is something that typifies doubly magic nuclei. Notice, however, that the effect is smaller for the exotic  $^{42}\text{Si}$ . A similar evidence comes from the  $1f_{7/2}$  occupation numbers along N=28. Those, shown in figure 14, reveal an increase of the  $f_{7/2}$  occupation at Z=20 and Z=14, again slightly in  $^{42}\text{Si}$ .

The  $2^+$  excitation energies of the isotopes of Ar and S, around N=28, are presented fig. 15 and compared with the corresponding energies of nuclei much closer to the stability at those neutron numbers (Ti, Cr). There is an upward shift of the excitation energies at N=28 that is a little smaller in Ar and S. The behaviour is seen to be very similar close and far off stability, thus indicating that the N=28 closure stands in the very neutron rich region.

From the analysis of these three sets of results:  $S_{2N}$ ,  $E_x(2^+)$  and the occupation numbers we can conclude that the  $1f_{7/2}^8$  neutron configuration at N=28, although somewhat eroded by the large neutron excess, is still dominant and that  $^{42}\text{Si}$  is a new doubly magic nuclei. Therefore, the vanishing of the shell closure far from stability that happens at N=20, does not seem to occur at N=28.

## C. The deformed nuclei $^{40}\text{S}$ and $^{42}\text{S}$

Our calculations show the existence of low lying  $2^+$  states for the Ar and S isotopes with  $22 \leq N \leq 26$ . However, only the Sulphur isotopes have large (and negative) spectroscopic quadrupole moments and enhanced E2 transitions (see figs. 18 and 19).  $^{42}\text{Ar}$  and  $^{44}\text{Ar}$  have reasonably large BE2's but very small spectroscopic quadrupole moments.

The lowest  $2^+$  energies correspond to  $^{40}\text{S}$  and  $^{42}\text{S}$ . Their spectroscopic quadrupole moments are  $-17.1\text{e}^2\text{fm}^2$  and  $-19.2\text{e}^2\text{fm}^2$  respectively. Assuming that the Bohr-Mottelson formula for the intrinsic quadrupole moment is applicable, we get  $Q_0=59.8\text{e}^2\text{fm}^2$  for  $^{40}\text{S}$  and  $Q_0=67.2\text{e}^2\text{fm}^2$  for  $^{42}\text{S}$ , corresponding to deformation parameters  $\beta \simeq 0.29$  and  $\beta \simeq 0.32$ . Our results are consistent with the Relativistic Mean Field calculations of Werner *et al.*, which predict  $\beta \simeq 0.25$ . Their non-relativistic calculations point to a more complicated situation with nearly degenerate prolate ( $\beta \simeq 0.25$ ) and oblate ( $\beta \simeq -0.24$ ) solutions. The only indication of coexistence in our results is provided by the presence of a very low (1.51 MeV) second  $0^+$  state in  $^{44}\text{S}$ .

The values of the E2 reduced transition probabilities are  $77.9\text{e}^2\text{fm}^4$  (A=40) and  $93.0\text{e}^2\text{fm}^4$  (A=42). We compare the quadrupole moments of  $^{42}\text{S}$  and other nuclei near N=28 in figure 14. The value for  $^{42}\text{S}$  is about 2/3 of that predicted for  $^{48}\text{Cr}$  leading to very similar deformation parameters  $\beta = 0.32$  and  $\beta = 0.30$ . In addition, the yrast levels of  $^{42}\text{S}$  follow the rotational law  $J(J+1)$  up to  $J=6$ .

It is also important to notice that, although a truncated  $1f_{7/2} 2p_{3/2}$  valence space for the neutrons, contains the basic degrees of freedom for the description of deformed nuclei in this region, it enhances either the rotational behaviour or the closed shell features, depending on the basic configurations that are involved. As an example let consider the evolution of the  $2^+$  excitation energies of the Sulphur isotopes. In the truncated space the energy of the  $2^+$  in N=26 goes down 200 keV to 0.88 MeV while in N=28 it goes up 300 keV to 1.78 MeV.

In order to explain the onset of deformation we shall explore which are the configurations that are responsible for the quadrupole coherence in our space. It is well known that the SU(3) symmetry is broken by the strong  $\vec{l} \cdot \vec{s}$  coupling in the pf shell. Yet, it has been recently shown [16] that the subspaces of a major shell spanned by  $\Delta j = 2$  orbits develop an approximate SU(3) symmetry, named quasi-SU(3). For instance the  $1f_{7/2} 2p_{3/2}$  valence space is enough to explain the collective behaviour of nuclei in the pf shell. In this space the maximal quadrupole collectivity is obtained for configurations with 4 protons and 4 neutrons. In our case, the basic neutron degrees of freedom are contained in this space, but protons are confined in the sd shell. For the nuclei we are interested in, the orbit  $1d_{5/2}$  is essentially closed and only the  $1d_{3/2}$  and the  $2s_{1/2}$  can be considered active. In this situation neither SU(3) nor quasi-SU(3) can develop.

However, one must look more carefully at the behaviour of these two orbits. As far as the neutrons are filling the sd shell, both orbits remain well separated. For instance, the excitation energy of the  $3/2_1$  level in  $^{29}\text{P}$  and  $^{35}\text{P}$  are 1.39 and 2.62 MeV respectively. Thus, the ground state wave functions are dominated by configurations with the

maximum allowed number of particles in the  $2s_{1/2}$  orbit. Particularly, for  $^{36}\text{S}$  the  $(2s_{1/2})^4$  configuration represents the 89% of the wave function. When the neutrons begin to fill the  $pf$  shell, the two orbitals become more and more degenerate (see table I) inducing strong mixing in the wave functions. A valence space with degenerate  $1d_{3/2}$  and  $2s_{1/2}$  orbitals has the geometry of pseudo-SU(3), and maximal quadrupole coherence is obtained for two protons, i.e. for the Sulphur isotopes. For three particles the quadrupole moment is strictly zero and beyond it changes of sign leading to oblate shapes. Thus, we expect other nuclei as, for instance, the Ar isotopes to have small collectivity.

Notice, however, that strict degeneration is achieved only at  $N=28$ , where the neutron collectivity is rather small. In other words, there is a mismatch between the region where protons have collective wave functions ( $N=28$ ) and the region where neutrons have quadrupole collectivity, that prevents the existence of a larger region of deformation. A compromise seems to take place for  $Z=16$  and  $N=26$  ( $^{42}\text{S}$ ) or  $N=24$  ( $^{40}\text{S}$ ).

#### IV. SUMMARY

In this paper we have studied the  $N=28$  region far from the stability. We have built an effective interaction for  $sd$  active protons and  $pf$  active neutrons that is the natural generalization of successful  $sd$ -only and  $pf$ -only interactions. The agreement of the theoretical results and the experimental data is very satisfactory. However, much more experimental information is needed to obtain a complete understanding of the region. Accurate information on the  $2^+$  excitation energies, on the evolution of the  $3/2^+, 1/2^+$  doublet along the Cl and P chains, the single particle spectrum of  $^{35}\text{Si}$  are challenges for the physics of exotic nuclei. We have also addressed the question of the magicity of  $N=28$ . A detailed analysis of the  $S_{2n}, 2^+$  energies and occupation numbers allow us to conclude that it persists in the very neutron rich regime, contrary to what happens at  $N=20$ . Finally our results show that the  $^{40,42}\text{S}$  isotopes are well deformed, but the effect seems to be very local; no large region of deformation is therefore expected.

**Acknowledgements.** We want to thank A. Zuker his decisive help in the determination of the effective interaction and G. Walter for enlightening discussions. This work has been partially supported by the IN2P3(France)-CICYT(Spain) agreements and by DGICYT (Spain) grant PB93-263.

- [1] C. Thibault *et al.* Phys. Rev. C **12** 193 (1975).
- [2] C. Detraz, D. Guillemaud, G. Huber, R. Klapisch, M. Langevin, F. Naulin, C. Thibault, L. C. Carraz and F. Touchard, Phys. Rev. C **19** 171 (1978).
- [3] G. Huber, F. Touchard, S. Buttenbach, C. Thibault, R. Klapisch, H. T. Duong, S. Liberman, J. Pinard, J. L. Vialle, P. Juncar and P. Jacquinet, Phys Rev C **18** 2342 (1978).
- [4] D. Guillemaud, C. Detraz, M. Langevin, F. Naulin, M. de Saint-Simon, C. Thibault, F. Touchard and M. Epherre, Nucl Phys A **246** 37 (1984).
- [5] A. Poves and J. Retamosa, Phys. Lett B **184** 311 (1987). A. Poves and J. Retamosa, Nucl. Phys A **571** 221 (1994).
- [6] E. K. Warburton, J. A. Becker and B. A. Brown, Phys. Rev. C **41** 1147 (1990).
- [7] N. Fukunishi, T. Otsuka, and T. Sebe, Phys. Lett. B **296** 1992 279.
- [8] X. Campi, H. Flocard, A. K. Kerman and S. Koonin, Nucl. Phys. A **251** 193 (1975).
- [9] O. Sorlin *et al.*, Phys. Rev. C **47** 2941 (1994).
- [10] H. V. Klapdor, J. Metzinger and T. Oda, At. Nucl. Data Tables **31**, 81 (1984).
- [11] A. Staudt, E. Bender, K. Muto and H. V. Klapdor, At. Nucl. Data Tables **44**, 1 (1990).
- [12] P. Möller and J. R. Nix, At. Data Tables **39**, 213 (1988).
- [13] P. Möller and J. R. Nix, Proceedings of the 6th Conference on Nuclei Far from Stability, Bernkastel-Kues, Germany, 1992.
- [14] J. M. Pearson, Y. A. Aboussir, A. K. Dutta, R. C. Navak, M. Farine and F. Tondeur, Nucl. Phys. A **258**, 1 (1991).
- [15] T. R. Werner, J. A. Sheikh, W. Nazarewicz, M. R. Strayer, A. S. Umar and M. Misu, Phys. Lett. B **335** 259 (1994).
- [16] A. Zuker, J. Retamosa, A. Poves and E. Caurier, Phys. Rev. C **52**, R1741 (1995).
- [17] A. Abzouzi, E. Caurier and A. Zuker, Phys. Rev. Lett. **66** (1991) 1134
- [18] G. Walter, Proc. Workshop on nuclear structure of light nuclei far from stability: Experiment and theory, ed. G. Klotz, C.R.N., Obernai (1990) p. 71
- [19] B. H. Wildenthal, M. S. Curtin and B. A. Brown, Phys. Rev. C **28**
- [20] A. Poves and A. Zuker, Phys. Rep. **70**,4 (1981).
- [21] S. Kahana, H. C. Lee and C. K. Scott, Phys. Rev. **180**, 956 (1969).
- [22] J. Duflo and A. P. Zuker, Phys. Rev. C **52**, R1 (1995).

- [23] A. Pape and M. S. Antony, *At. Data Nucl. Data Tables* 39 (1988)
- [24] E. Caurier, A. P. Zuker, A. Poves and G. Martínez-Pinedo, *Phys. Rev. C* **50** 225 (1994).
- [25] E. Caurier, code ANTOINE, Strasbourg (1989).
- [26] R. R. Whitehead, in *Moments Methods in Many Fermion Systems*, edited by B. J. Dalton, S. M. Grimes, J. D. Vary and S. A. Williams (Plenum, New York, 1980), p. 235.
- [27] D. H. Wilkinson and B. E. F. Macefield, *Nucl. Phys. A* **232**, 58 (1974).
- [28] *Table of Isotopes* (7th edition), Eds. C. M. Lederer and V. S. Shirley (1978).
- [29] G. Audi and A. H. Wapstra, *Nucl. Phys. A* **565**, 1 (1993)

TABLE I.  $2_1^+$  excitation energies (in MeV).

	$N$	22	24	26	28	30
<i>Cr</i>	<i>th</i>	0.869	0.742	0.793	1.621	0.877
	<i>exp</i>	0.869	0.751	0.783	1.434	0.835
<i>Ti</i>	<i>th</i>	1.209	0.869	1.003	1.755	1.103
	<i>exp</i>	1.083	0.889	0.983	1.555	1.047
<i>Ca</i>	<i>th</i>	1.534	1.409	1.338	3.947	1.110
	<i>exp</i>	1.524	1.157	1.347	3.832	1.030
<i>Ar</i>	<i>th</i>	1.368	1.249	1.182	1.655	1.219
	<i>exp</i>	1.461	1.208	–	–	–
<i>S</i>	<i>th</i>	1.209	1.047	1.073	1.465	1.272
	<i>exp</i>	–	–	–	–	–
<i>Si</i>	<i>th</i>	1.900	1.670	1.652	2.558	1.461
	<i>exp</i>	–	–	–	–	–

TABLE II. Energy difference between the  $3/2_1^+$  and  $1/2_1^+$  states in K, Cl and P.

	$N$	20	22	24	26	28	30
<i>K</i>	<i>th</i>	2.73	0.96	0.67	0.28	-0.38	0.19
$E(1/2) - E(3/2)$	<i>exp</i>	2.52	0.98	0.56	0.47	-0.36	–
<i>Cl</i>	<i>th</i>	1.82	0.71	0.06	-0.21	-0.05	-0.06
$E(1/2) - E(3/2)$	<i>exp</i>	1.73	0.40	–	–	–	–
<i>P</i>	<i>th</i>	2.61	1.32	0.68	0.32	0.06	0.38
$E(3/2) - E(1/2)$	<i>exp</i>	–	–	–	–	–	–

TABLE III. Total Gamow-Teller strength and theoretical vs. measured half-lives of the even-even Ar and S isotopes.

	$GT^-$	$T_{\frac{1}{2}}^{th}$	$T_{\frac{1}{2}}^{exp}$
$^{44}\text{Ar}$	22.85	4.70m	11.87m
$^{46}\text{Ar}$	28.84	6.94s	8.4s
$^{38}\text{S}$	16.78	174.4m	170.3m
$^{40}\text{S}$	22.87	6.67s	8.8s
$^{42}\text{S}$	28.89	389ms	560ms
$^{44}\text{S}$	34.93	54ms	123ms

FIG. 1. Theoretical and experimental natural parity states for  $^{40}\text{K}$

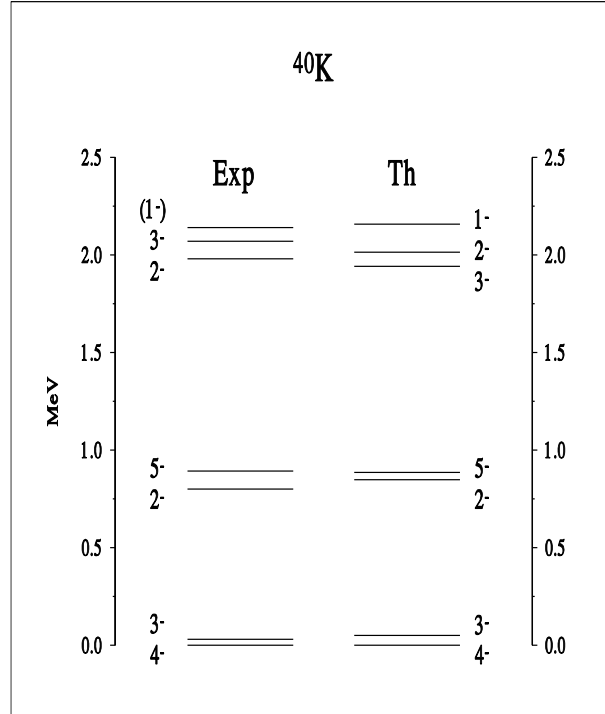


FIG. 2. Same as figure 1 for  $^{41}\text{K}$

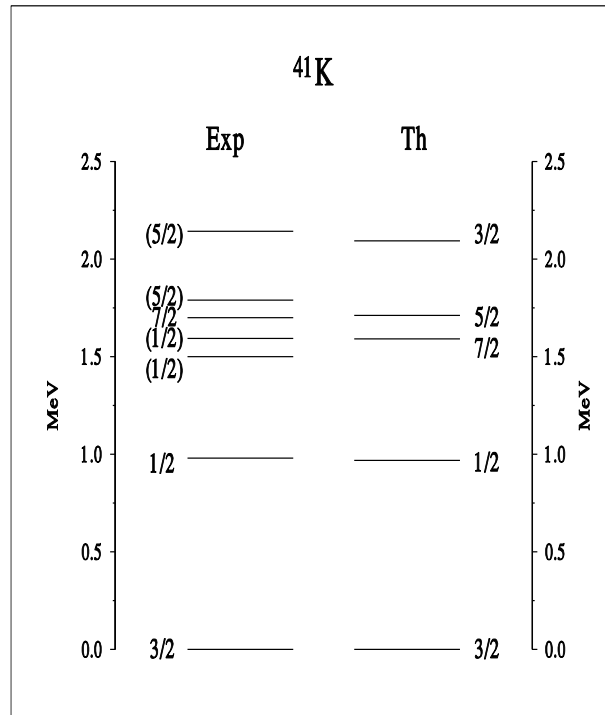


FIG. 3. Same as figure 1 for  $^{42}\text{K}$

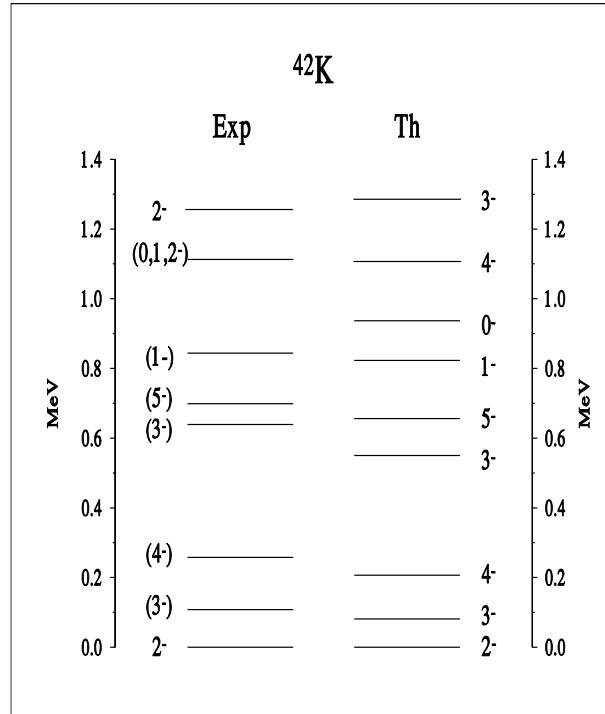


FIG. 4. Same as figure 1 for  $^{39}\text{Ar}$

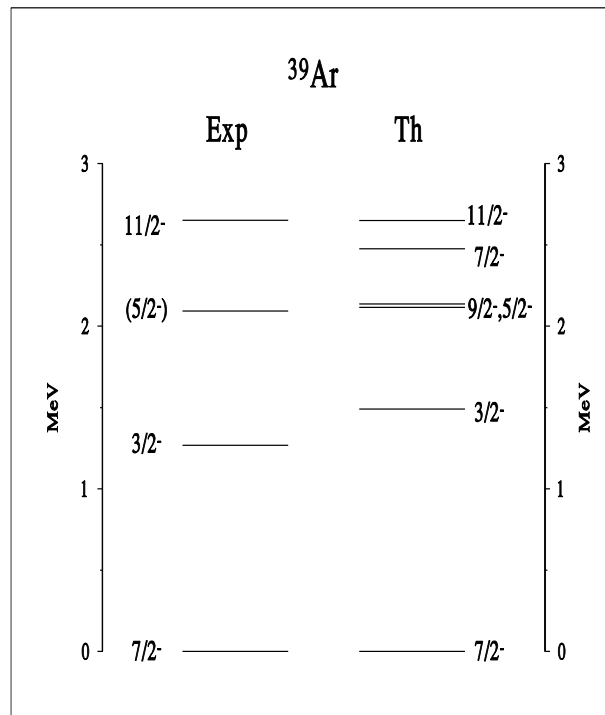


FIG. 5. Same as figure 1 for  $^{40}\text{Ar}$

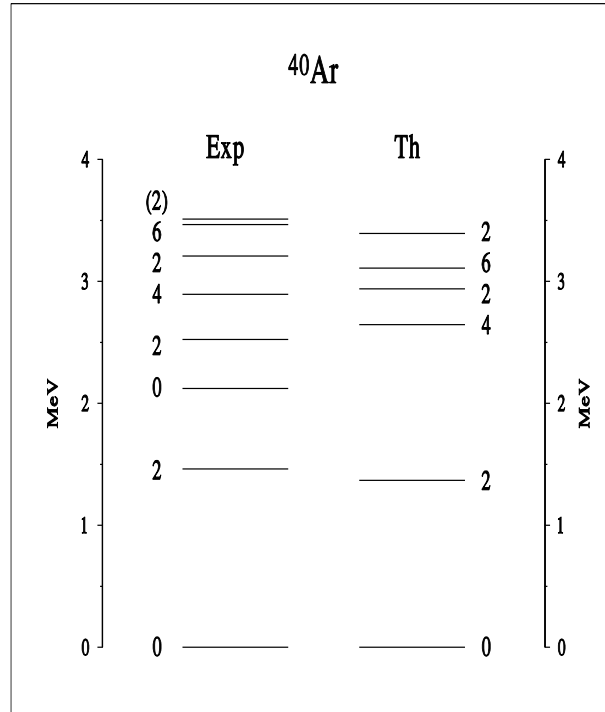


FIG. 6. Same as figure 1 for  $^{41}\text{Ar}$

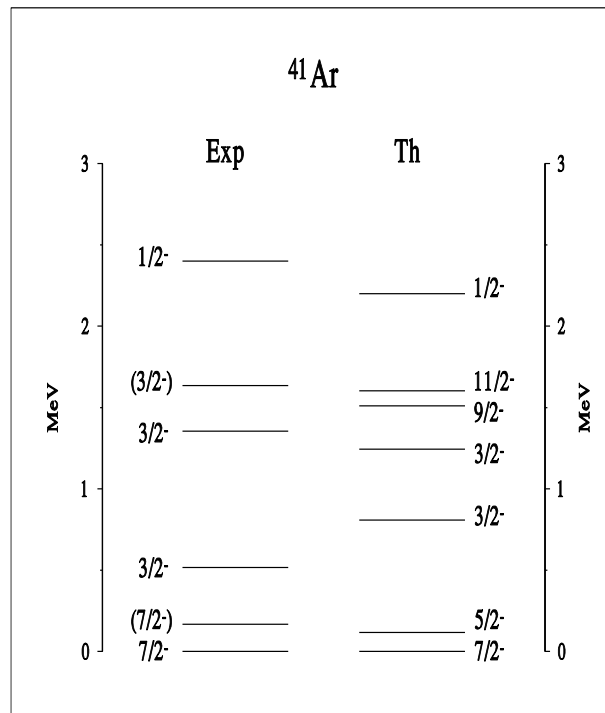


FIG. 7. Same as figure 1 for  $^{38}\text{Cl}$

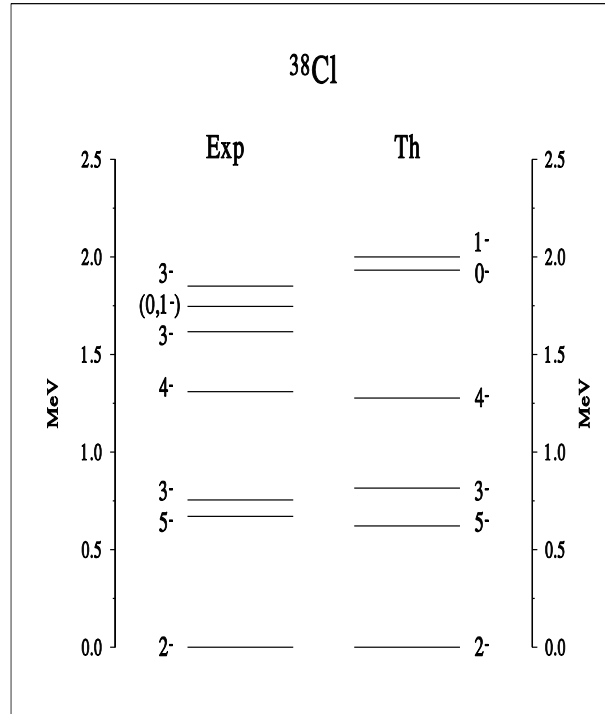


FIG. 8.  $S_{2n}$  energies for the Ca isotopes.

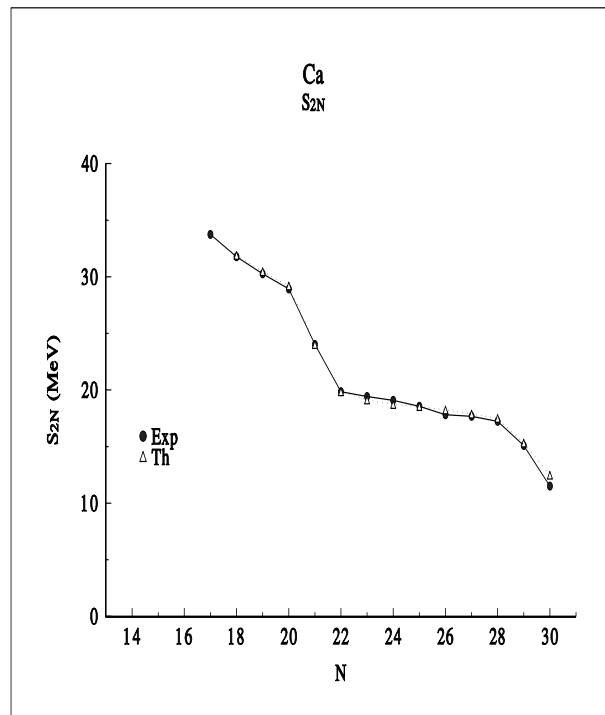


FIG. 9.  $S_{2n}$  energies for the K isotopes.

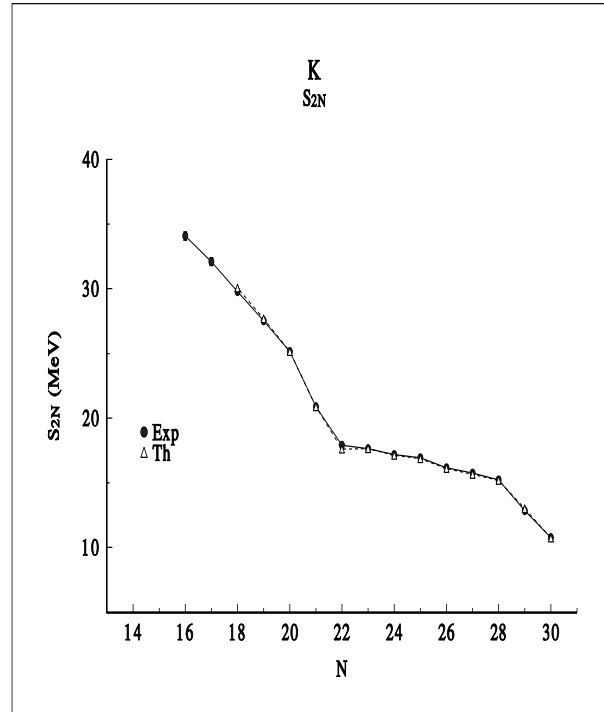


FIG. 10.  $S_{2n}$  energies for the Ar isotopes. The experimental points at the vertical line beyond are not measured quantities but numbers from Audi and Wapstra's extrapolations

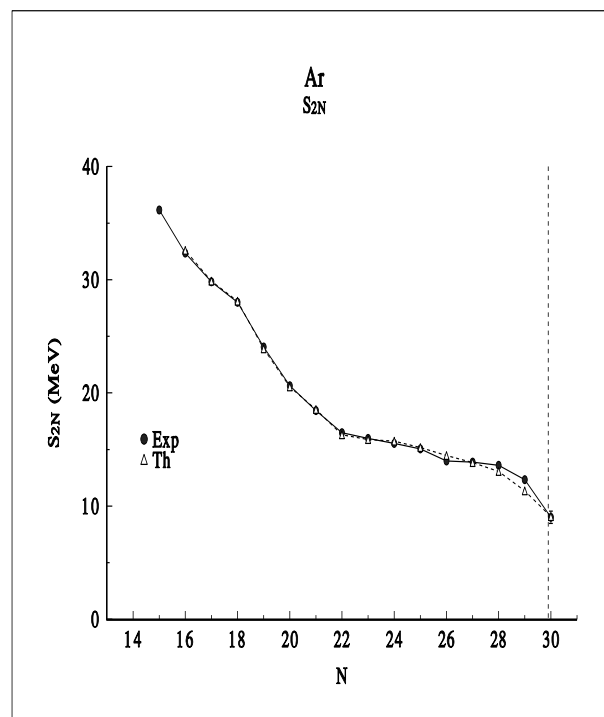


FIG. 11.  $S_{2n}$  energies for the Cl isotopes. See caption to figure 10.

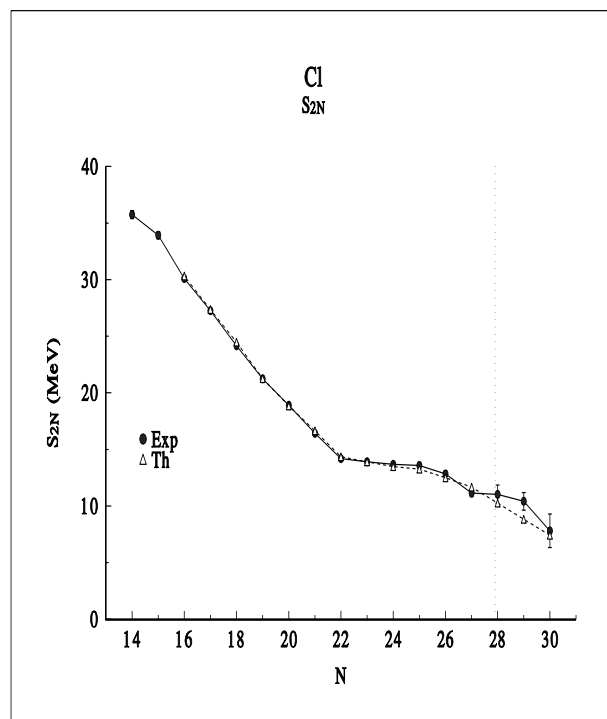


FIG. 12.  $S_{2n}$  energies for the S isotopes. See caption to figure 10.

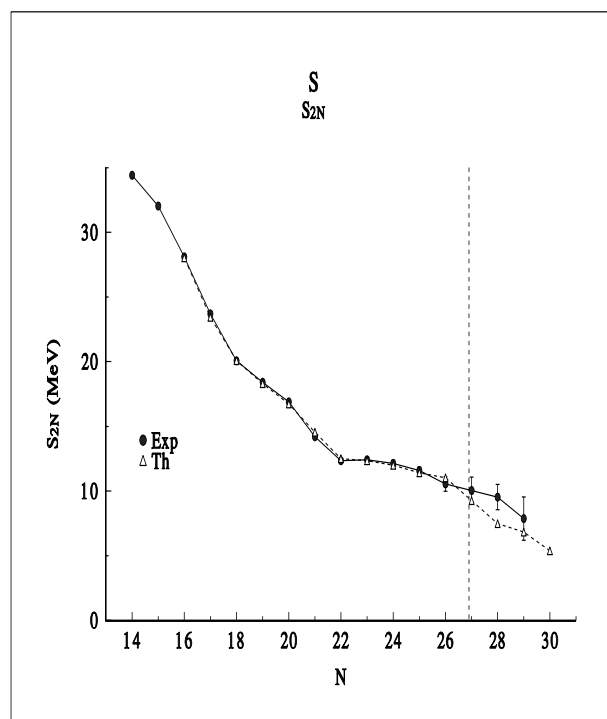


FIG. 13.  $S_{2n}$  energies for the P isotopes. See caption to figure 10.

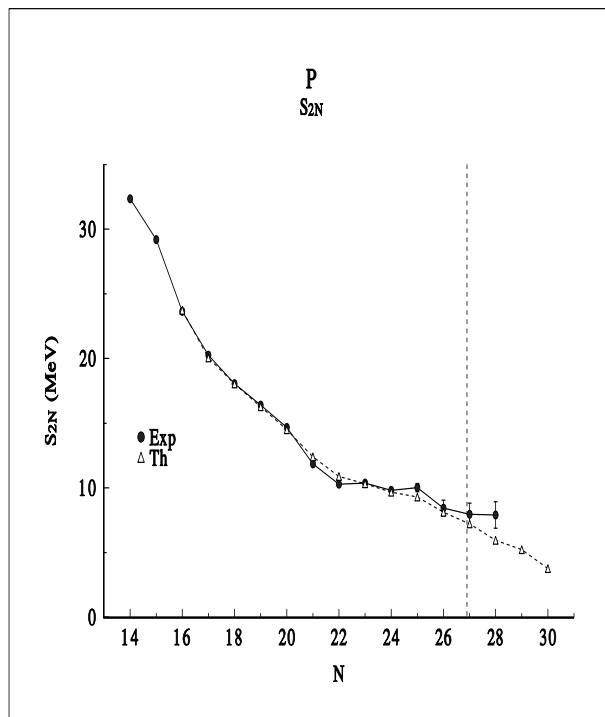


FIG. 14.  $S_{2n}$  energies for the Si isotopes. See caption to figure 10.

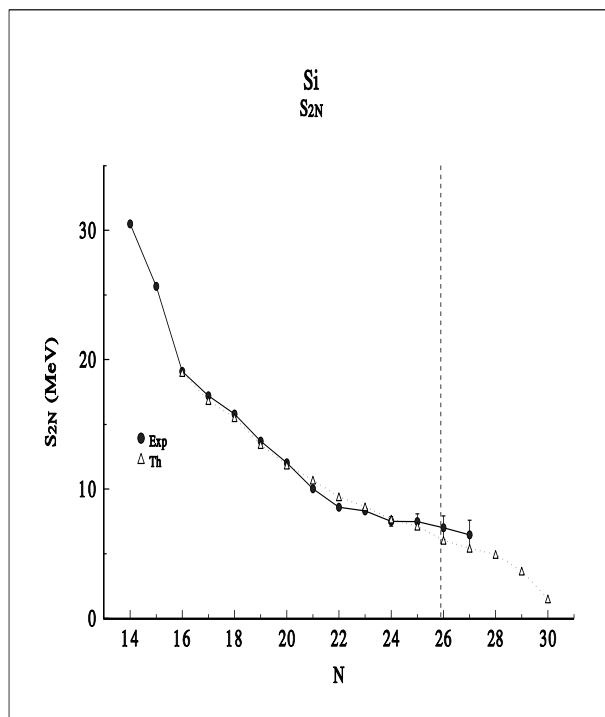


FIG. 15.  $2^+$  excitation energies for the Ca and Si isotopes.

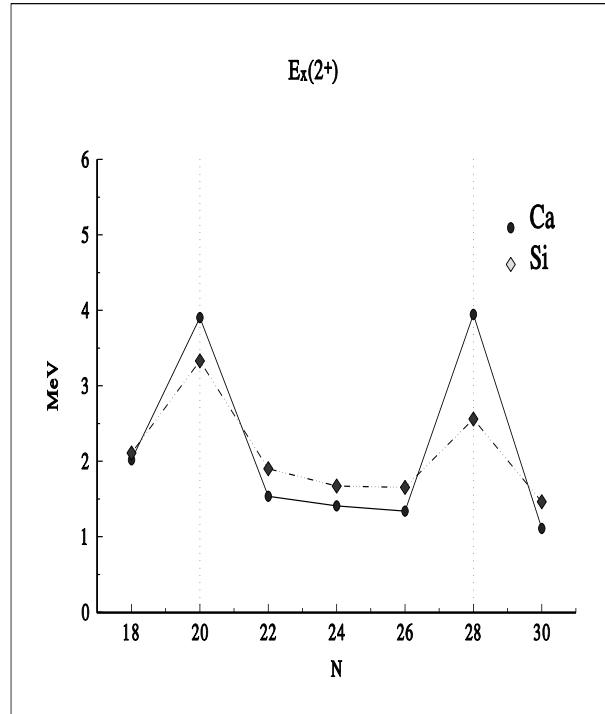


FIG. 16.  $2^+$  excitation energies for the Ca and Si isotopes.

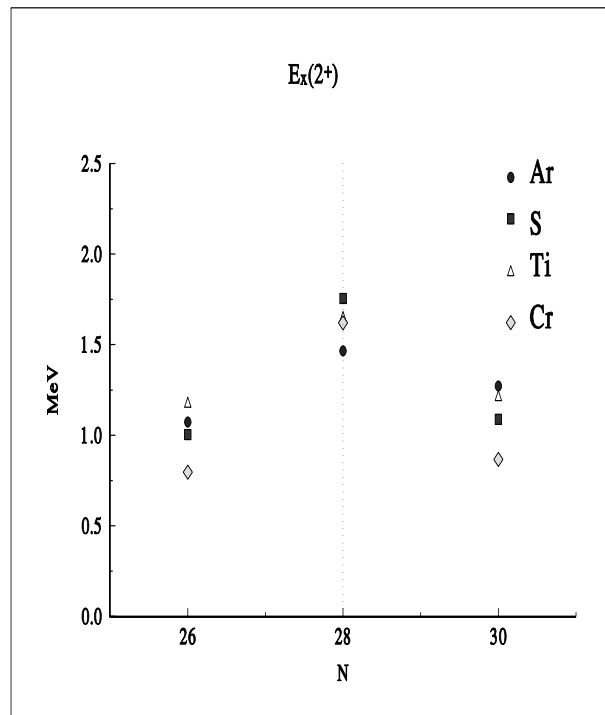


FIG. 17.  $f_{7/2}$  occupation numbers.

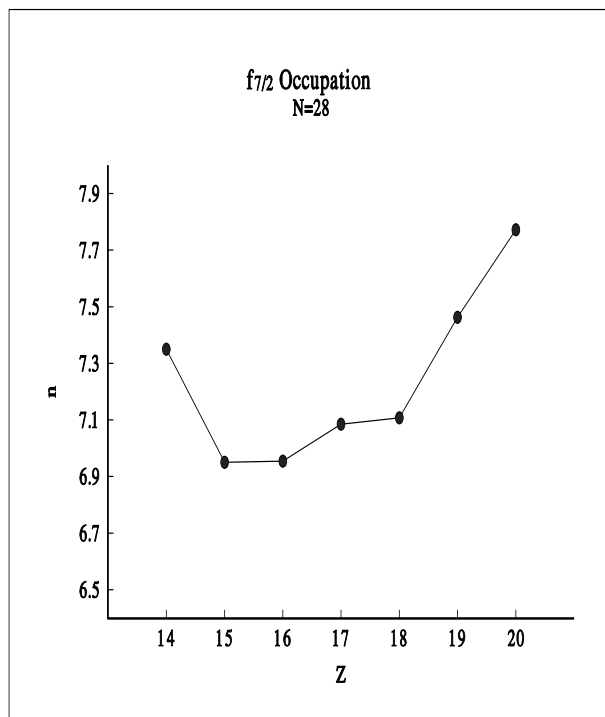


FIG. 18. Spectroscopic Quadrupole moments for the Cr, Ti, Ar and S isotopes.

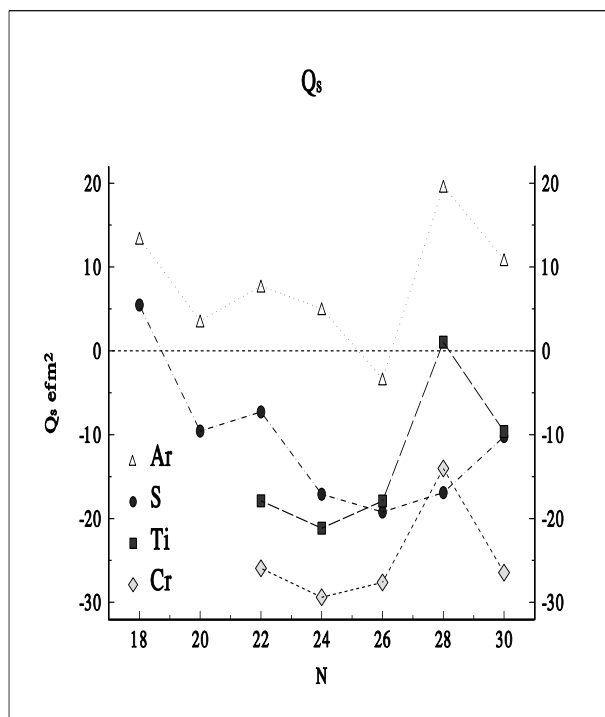
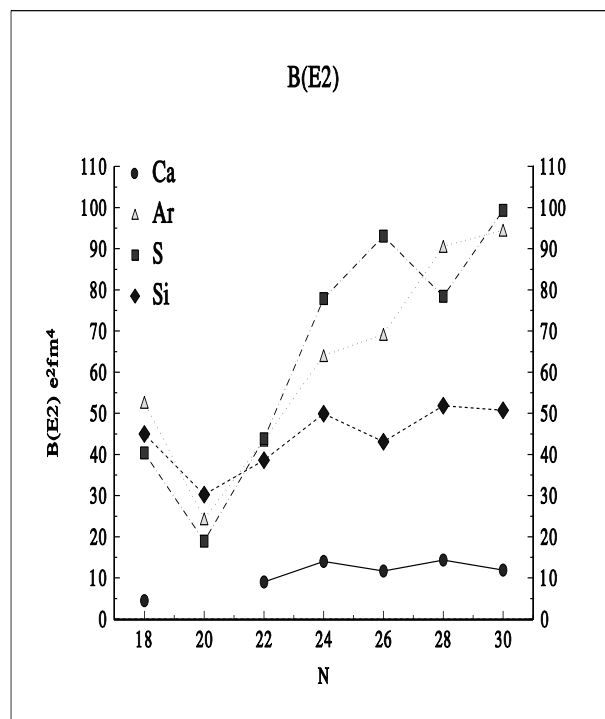


FIG. 19. BE2 for Ca, Ar, S and Si isotopes.



$^{42}\text{Ar}$

Exp

Th

